Journal of Structural Geology 32 (2010) 1899–1911

Contents lists available at ScienceDirect

Journal of Structural Geology

journal homepage: www.elsevier.com/locate/jsg

Fault-related clay authigenesis along the Moab Fault: Implications for calculations of fault rock composition and mechanical and hydrologic fault zone properties

John G. Solum [a,*], Nicholas C. Davatzes [b], David A. Lockner [c]

[a] Shell International Exploration and Production, Inc., Bellaire Technology Center, 3737 Bellaire Blvd., Houston, TX 77025, USA
[b] Department of Earth and Environmental Science, Temple University, 326 Beury Hall, 1901N. 13th Street, Philadelphia, PA 19122, USA
[c] U.S. Geological Survey, Earthquake Hazards Team, 345 Middlefield Rd MS 977, Menlo Park, CA 94025, USA

ARTICLE INFO

Article history:
Received 10 August 2009
Received in revised form
13 July 2010
Accepted 28 July 2010
Available online 26 October 2010

ABSTRACT

The presence of clays in fault rocks influences both the mechanical and hydrologic properties of clay-bearing faults, and therefore it is critical to understand the origin of clays in fault rocks and their distributions is of great importance for defining fundamental properties of faults in the shallow crust. Field mapping shows that layers of clay gouge and shale smear are common along the Moab Fault, from exposures with throws ranging from 10 to ~1000 m. Elemental analyses of four locations along the Moab Fault show that fault rocks are enriched in clays at R191 and Bartlett Wash, but that this clay enrichment occurred at different times and was associated with different fluids. Fault rocks at Corral and Courthouse Canyons show little difference in elemental composition from adjacent protolith, suggesting that formation of fault rocks at those locations is governed by mechanical processes. Friction tests show that these authigenic clays result in fault zone weakening, and potentially influence the style of failure along the fault (seismogenic vs. aseismic) and potentially influence the amount of fluid loss associated with coseismic dilation. Scanning electron microscopy shows that authigenesis promotes that continuity of slip surfaces, thereby enhancing seal capacity. The occurrence of the authigenesis, and its influence on the sealing properties of faults, highlights the importance of determining the processes that control this phenomenon.

1. Introduction

Clays are common constituents of fault rocks, and affect both the mechanical and hydrologic properties of the faults that contain them. Most clay minerals are mechanically weak, and so the type and amount of clay minerals in fault rocks can influence the frictional fault strength (Morrow et al., 2007; Tembe et al., 2006). The frictional strength of rock can be reduced from nominal values of 0.6–1 in quarto-feldspathic rocks to <0.3 with as little as 18% clay (Tembe et al., 2006). In addition, clay minerals have a range of rate dependences of the coefficient of friction, ranging from positive values that favor creep to negative values that favor seismic slip (Saffer and Marone, 2003; Lockner et al., 2006). Similarly, permeability can be reduced as much as seven orders of magnitude due to the incorporation of clay in fault rocks (Crawford et al., 2002; Davatzes and Hickman, 2005). Thus the occurrence of clay-rich fault rocks tends to dominate fault zone hydrologic properties such as permeability and transmissibility and their anisotropy (Solum and van der Pluijm, 2009; Walsh et al., 1998, 2002; Faulkner and Rutter, 2001; Fisher and Knipe, 2001; Manzocchi et al., 1999; Knipe et al., 1998; Yielding et al., 1997; Aydin and Eyal, 2002) and capillary entry pressure, which controls fault seal capacity (Sperrevik et al., 2002; Bretan et al., 2003). As the clay concentration in fault rocks increases the permeability decreases and the capillary entry pressure increases.

Given the role clays play in influencing fault behavior, their concentration in fault zones and the governing mechanisms controlling that concentration must be quantified. Two commonly used empirical methods of estimating the clay concentration in fault rocks are the shale gouge ration (SGR) (Yielding et al., 1997) and the clay smear potential (CSP) (Fulljames et al., 1997). The SGR approach calculates clay concentrations based on the assumption that the gouge composition at a particular point along a fault is equivalent to the geometrically averaged composition of all of the host rock that has moved past that point, implying mixing of the various rock bodies offset by the fault. The CSP approach is based on the assumption that clay-rich horizons will be smeared into a fault, with the offset over which the smear remains continuous and its thickness are taken as a function of the thickness of the clay beds

* Corresponding author. Tel.: +1 713 245 7787; fax: +1 713 245 7532.
E-mail address: j.solum@shell.com (J.G. Solum).

0191-8141/$ – see front matter © 2010 Elsevier Ltd. All rights reserved.
doi:10.1016/j.jsg.2010.07.009

and the offset of the fault. In this scenario, fault rock is wholly a product of shale source beds without mixing with other rock types until the critical offset is reached at which point the smear "breaks". Since it is possible to empirically relate clay content to permeability or membrane sealing capacity through laboratory measurement or in situ pressure differences across faults, it is possible to use CSP and/or SGR to estimate fault rock permeability and transmissibility. Neither CSP nor SGR calculations account for fault-related clay authigenesis, which can be a significant source of clay or alter the physical properties of the clay including porosity, shear strength (friction), and permeability.

Studies over the past decade have shown that fault-related clay authigenesis is a common process in fault zones in a variety of geologic settings: the San Andreas Fault (Solum et al., 2006; Schleicher et al., 2006; Tembe et al., 2006; Morrow et al., 2007), thrust faults in the North American Cordillera (Vrolijk and van der Pluijm, 1999; Yan et al., 2001; van der Pluijm et al., 2001, 2006; Solum and van der Pluijm, 2007), a small normal fault in northern California (Eichhubl et al., 2006), and along the Moab Fault in Utah (Solum et al., 2005; Pevear et al., 1997; Anyamele et al., 2009).

In addition to the generation of fault rock, fault zone hydrology is greatly impacted by small-scale structures within the damage zone (Caine et al., 1996), which are distributed adjacent to the fault rock and vary by position (Davatzes et al., 2005a,b) and lithology. The damage zone consists of a region of enhanced deformation adjacent to the core of fault rock. Its impact on fault zone hydrology depends on the type and distribution of structures within the zone (including joints, fractures, deformation bands, and folds) their geometric and age relationships, and the spatial variation in the width of the damage zone along the fault.

It is not possible to adequately image either the attributes of the damage zone and the fault rock either through seismic methods or even with wells due to limited sampling, and so their nature must be predicted, but predictive relationships are generally lacking. In addition, both the damage zone and the fault rock attributes vary in width along faults related to a number of parameters including the stratigraphic heterogeneity, early fault geometry (Childs et al., 2009), and the local state of stress, which are difficult to predict from the fully developed fault geometry in the subsurface visible in reflection seismic data. However, the physical mechanisms that account for the formation of clay-rich fault rocks, and the conditions under which such mechanisms operate, can be effectively investigated from outcrop analogues, providing a sound basis for predicting fault rock attributes. The Moab Fault is one such analogue.

The purpose of this study is to 1) describe the occurrence of clay-rich fault rocks along 4 exposures of the Moab Fault; 2) determine as best as possible the degree of authigenesis at each site; 3) speculate on more generally applicable ways in which this authigenesis may affect hydrologic and mechanical fault properties.

2. Geologic setting

The Moab Fault, located in eastern central Utah (Fig. 1), is a large normal fault that cuts a heterogeneous series of dominantly clastic sedimentary rocks (Fig. 2). The fault is composed of three main components, a poorly exposed southern section, a central section where the greatest throws (up to ~1 km) are found, and a complex branching northern section that tips out to the northwest. The fault was initially activated in the Early Mesozoic in response to motion of thick accumulations of salt deposited in the Pennsylvanian (Foxford et al., 1996, 1998; Doelling, 2001). The fault was reactivated at ~60 Ma (Solum et al., 2005), likely due to reinitiated salt movement during the Laramide Orogeny.

The architecture of this fault zone is variable, and has been studied by several authors. The first systematic study was conducted by Foxford et al. (1996, 1998), which classified architectural elements into slip band zones, shaley gouge zones, and sandstone cataclasites and breccias. While that study described many locations along the fault, it did not describe the geometry of the architectural

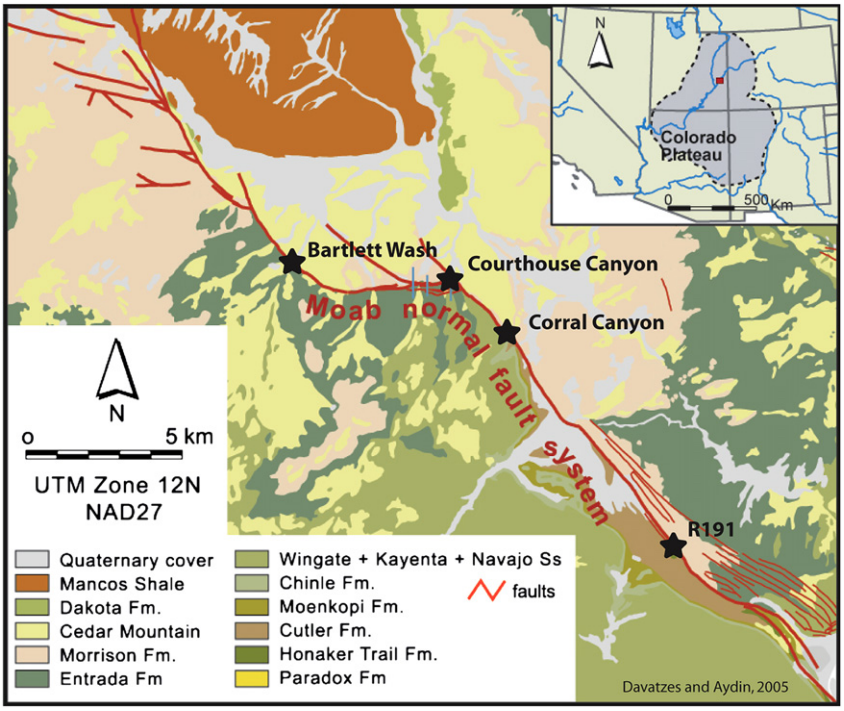

Fig. 1. Simplified geologic map of the Moab Fault system (Davatzes and Aydin, 2005) with sample locations noted. Locations are R191 (throw of ~960 m), Corral Canyon (throw of ~500 m), Courthouse Canyon (throw of ~10 m), and Bartlett Wash (throw of ~250 m).

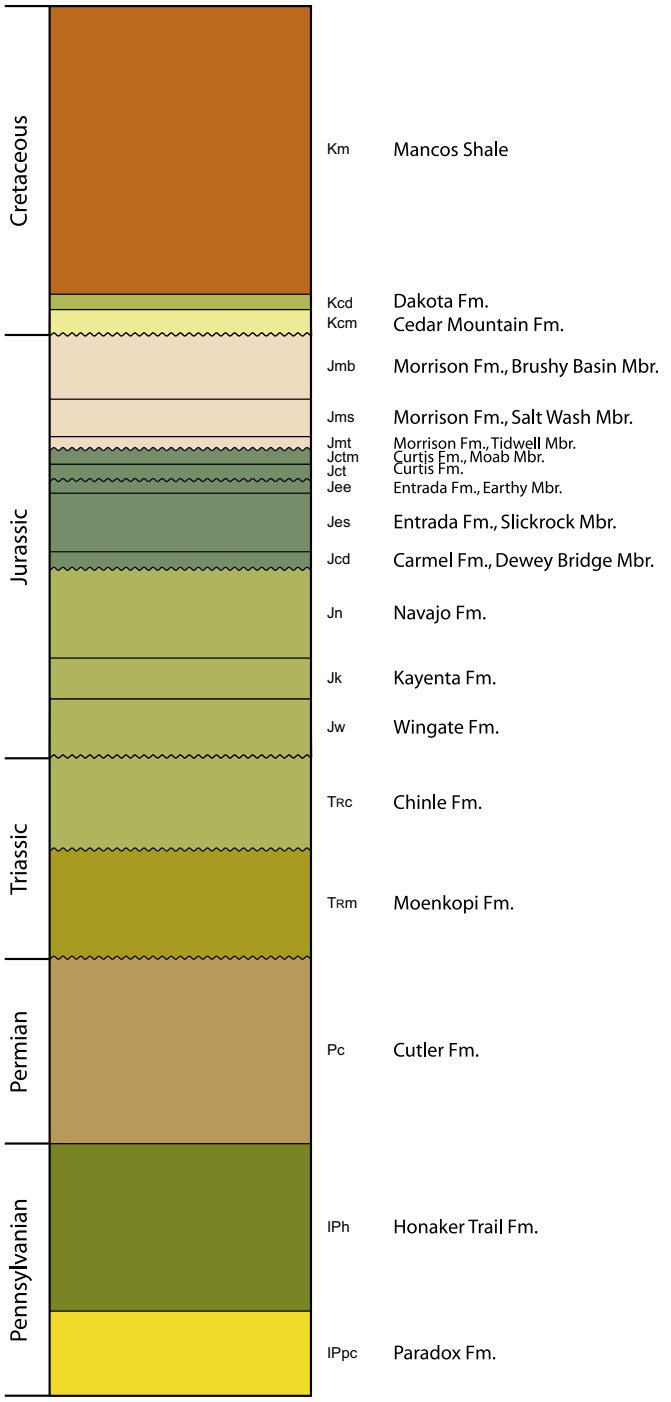

Fig. 2. Stratigraphy of the Moab area (modified from Doelling, 2001 and Davatzes and Aydin, 2005).

elements or subdivide the clay-rich fault rocks. Davatzes et al. (2005a,b) and Davatzes and Aydin (2005) characterized the geometry of these structures in the fault zone in more detail, explicitly mapping the geometries of the rocks surrounding the fault and their relationship to the larger fault geometry. Johansen et al. (2005) described the damage zone structures and their distribution, but confined themselves to sandstones.

Many studies have documented multiple episodes of fluid flow along the Moab Fault. The two major episodes of fluid flow can be described as follows:

1) Mineralization associated with a Ba–Sr bearing fluid (Morrison and Parry, 1986; Breit et al., 1990; Garden et al., 2001) that is also associated with Fe-reduction (Chan et al., 2000; Garden et al., 2001). The paleomagnetic pole position of remagnetized bleached sandstones associated with this reducing event indicates an age of 49–62 Ma (Garden et al., 2001), which coincides with late generation of hydrocarbons from the Ismay and Desert Creek members of the Paradox Formation in the Moab area at ~72–38 Ma (Nuccio and Condon, 1996). Based on direct dating of illite-bearing gouge the central section of the Moab Fault was active at 60–63 Ma (Solum et al., 2005). We therefore interpret Ba + Sr concentration as being controlled by fluids associated with hydrocarbon migration, and fault activity, in the Paleocene.
2) Mineralization associated with a Cu + Pb + Zn bearing fluids observed along the Moab Fault (Garden et al., 1996) and in the greater Moab area (Morrison and Parry, 1986), likely related to igneous activity in the nearby La Sal Mountains. Nelson et al. (1992) report K–Ar and $^{40}Ar/^{39}Ar$ ages of 27.9–25.1 Ma for alkali feldspars and hornblende from the La Sal Mountains. Chan et al. (2001) report a $^{40}Ar/^{39}Ar$ age of 20–25 Ma for cryptomelane, a potassium manganese oxide, in an exposure of the southern section of the Moab Fault, and associate its mineralization with fluids sourced from the La Sals. On the basis of those ages we interpret Cu + Pb + Zn concentrations as being associated with fluid migration in the Oligocene. There is evidence for fault activity in the greater Moab area at this time. Williams (2005) reports ages of 25–47 Ma based on direct dating of illite in fault gouge for activity along the Little Grand Wash Fault ~20 km NW of the northernmost Moab Fault.

Eichhubl et al. (2009) used field mapping and isotopic analyses of fault-related carbonates to infer that fluid flow along the Moab Fault was enhanced in areas of structural complexity, such as near fault intersections where joint formation and brecciation resulted from the mechanical interaction of fault segments (Davatzes et al., 2005a,b). These indications of widespread fault–fluid interactions highlight the importance of constraining the development of clay-rich fault rocks along the Moab Fault.

3. Methods and results

3.1. Clay-rich fault rocks along the Moab Fault

Clay-rich fault rocks are present at all locations (Figs. 3–8), with all locations containing both clay gouge and smear. For the purposes of this paper clay gouge is defined as a clay-rich fault rock the origin of which cannot be traced to a single formation. Smear is defined as fault rocks that can be traced to a particular formation, for example by tracing deformed and sheared beds away from the fault.

Foxford et al.'s (1996) R191 location (Fig. 3) is an exposure along the old route of Highway 191 near the location of maximum throw along the fault. This outcrop is located ~5 km northwest of the entrance to Arches National Park where the Permian Cutler Group and Pennsylvanian Honaker Trail Formation are juxtaposed against the Salt Wash member of the Jurassic Morrison Formation (throw of 960 m based on the work of Foxford et al., 1996, 1998). The fault zone here is comprised of two subparallel segments, a larger segment accommodating 900 m of throw, and a smaller with 60 m of throw. The gouge zone for the main fault is up to ~1 m wide, and is composed of bleached yellow gouge, bleached white/green gouge, and unbleached red gouge. This main gouge zone is bound by a layer of less-intensely deformed smear that is 3–4 m wide. Discontinuous sandstone beds within this smear can be traced to

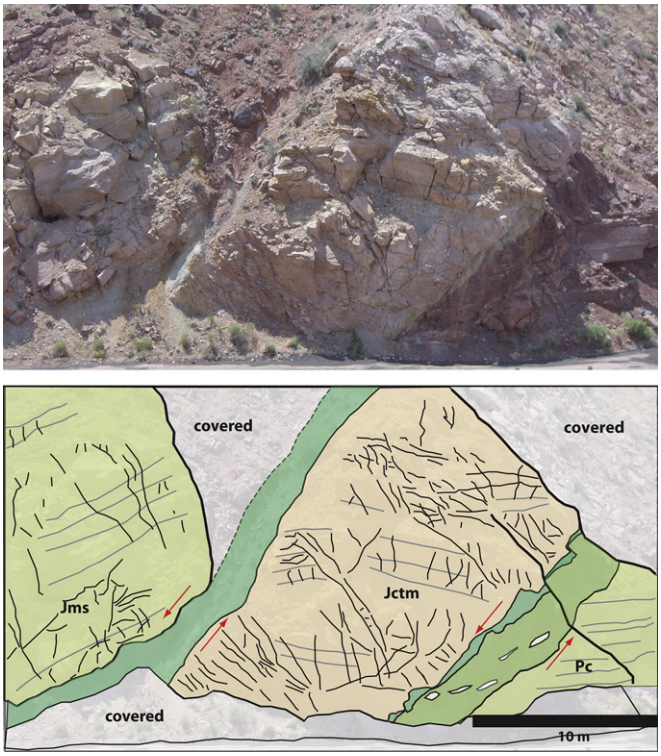

Fig. 3. Photograph and interpretation of the R191 location, the site of maximum throw along the fault. The protolithic Cutler formation in the footwall becomes a zone of Cutler-derived smear within a few meters of the fault, and this smear is in turn bound by an up to 1 m thick zone of clay gouge along a fault with a throw of 900 m. The protolithic Salt Wash Member of the Morrison Formation in the hanging wall abuts against a zone of smear derived from the Moenkopi Formation (not shown – see Foxford et al., 1998) and a minor gouge zone with a throw of ~60 m.

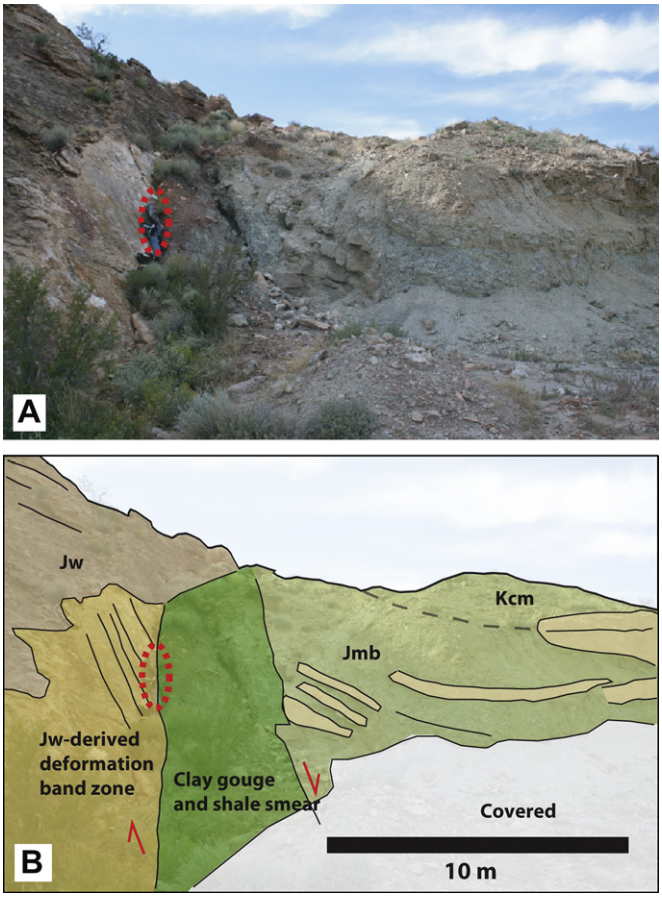

Fig. 4. Photograph and interpretation of the fault at Corral Canyon. At this location that fault accommodates ~500 m of throw. As at the R191 location there is a zone of shale smear. At this location the smear can clearly be traced to undeformed protolith (the Brushy Basin Member of the Morrison Formation) in the hanging wall of the fault. See Fig. 5 for a closer view of the gouge zone. A geologist is circled for scale.

undeformed beds in the adjacent Cutler Group, constraining the origin of the smear. The minor gouge zone is up to ~2 m wide, and is composed of bleached gouge. There is also a zone of smear derived from the Moenkopi Formation that is ~3 m wide.

The Corral Canyon exposure (Figs. 4 and 5) is located ~6 km north of the intersection of Highways 191 and 313. At this location the fault juxtaposes Wingate Sandstone against the clay-rich Brushy Basin member of the Morrison Formation and the Cedar Mountain Formation. The stratigraphic juxtaposition indicates a fault throw of ~500 m at this location (Foxford et al., 1998; Davatzes and Aydin, 2005). The main gouge zone at Corral Canyon is composed of two bands of gouge, one bleached and the other not, with a cumulative thickness of ~10 cm. This gouge zone transitions into a ~5 m thick layer of shale smear derived from the Brushy Basin member of the Morrison Formation in the hanging wall of the fault.

The Courthouse Canyon exposure (Fig. 6) is along the main section of the Moab Fault near where it begins to tip out, and where a branching northern section begins. The location sampled for this study is located in the footwall of the central section of the fault and shows a smaller fault that self juxtaposes the Tidwell Member. The amount of displacement on this fault is unclear but is on the order of ~10 m or less. Despite the small throw at this location there is a continuous ~1.5 cm thick layer of red gouge along the fault contact. There is a zone of smear ~0.3 m thick in the hanging wall of the fault.

The Bartlett Wash exposure (Figs. 7 and 8) occurs along the northern section of the fault, and is the only location along the northern section that is visited in this paper. At Bartlett wash the fault juxtaposes the Entrada and Curtis formations in the footwall against the Cedar Mountain and Morrison (Brushy Basin and Salt Wash) formations in the hanging wall indicating ~250 m of throw. There is also a smaller fault with a throw of ~15 m that juxtaposes the Moab Tongue member of the Curtis formation against itself. The gouge zone along the fault is ~0.15–0.5 m thick, and is composed of multiple zones of multicolored gouge (green and red, red, yellow, and red and white). There is a thick layer of

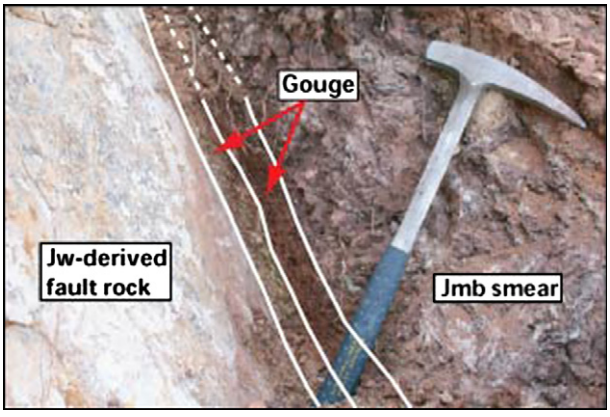

Fig. 5. Closer view of the gouge at Corral Canyon. In addition to the zone of shale smear described in Fig. 4 there is also a thin zone of clay gouge at this location.

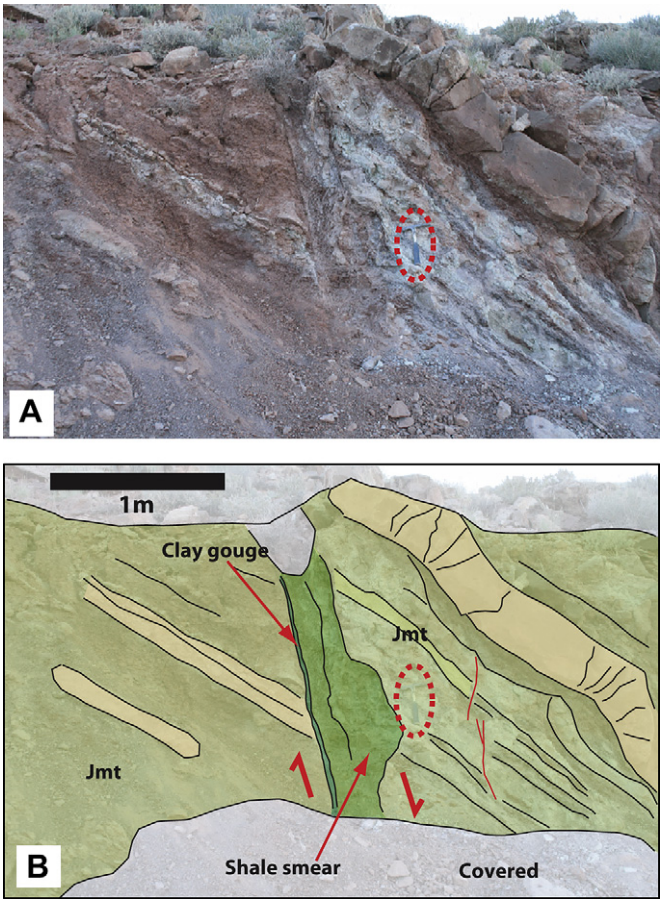

Fig. 6. Photograph and interpretation of the fault at Courthouse Canyon. This exposure is in the footwall of the main fault at this location. The main fault (not shown) has a throw of ~150 m, while this fault has a throw of ~10 m. Despite its relatively small offset this fault has a zone of shale smear and a very thin layer of clay gouge, broadly similar to that observed at the other locations along the fault. A geologic hammer is circled for scale.

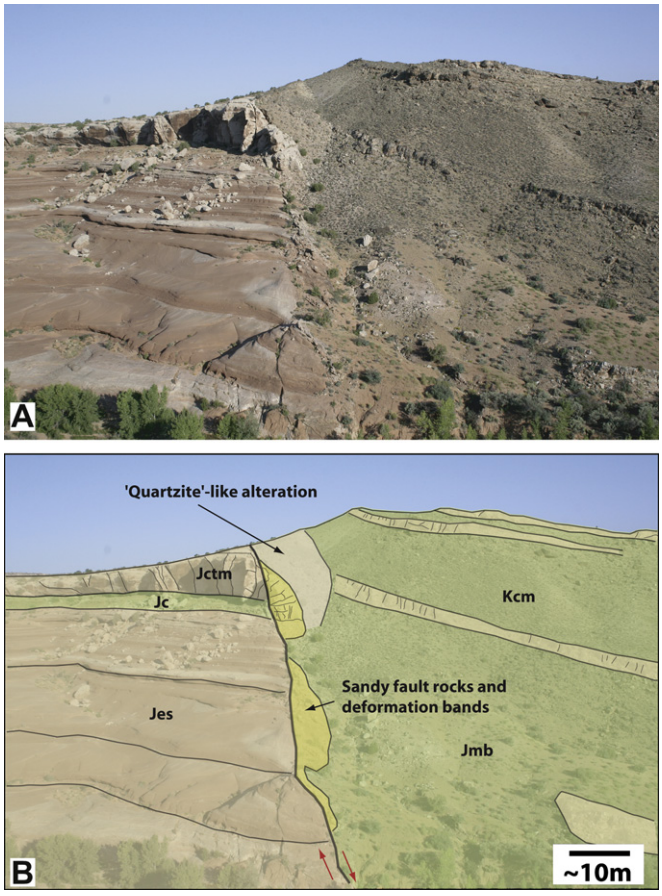

Fig. 7. Photograph and interpretation of the fault at Bartlett Wash. Closer view shown in Fig. 8. The fault system at this location is composed of two faults, a minor fault which self juxtaposes the Moab Tongue of the Curtis Formation and has a throw of ~15 m and a larger fault which juxtaposes the Cedar Mountain and Morrison Formations (Brushy Basin and Salt Wash Members) against the Curtis (Moab Tongue) and Entrada (Slick Rock) formations. As observed elsewhere along the fault (Davatzes and Aydin, 2005), there is a zone of shale smear that can be traced into undeformed protolith (Brushy Basin Member of the Morrison Formation).

smear 2+ m thick. The thickness of the smear is difficult to measure due to poor exposure.

3.2. Fluid flow along the Moab Fault

As discussed above there have been multiple fluid flow events in the greater Moab area since the formation of the Moab Fault in the Permo-Triassic. Barium and strontium are used as tracers for a Paleocene fluid flow event associated with a period of major activity and hydrocarbon migration along the Moab Fault and copper, lead and zinc are used as tracers for a younger Oligocene fluid flow event. Background concentrations of these elements were defined using previously published whole-rock X-ray fluorescence (XRF) analyses of the Cutler, Moenkopi, Chinle, Wingate, Kayenta, Navajo, Entrada, and Morrison formations (Breit et al., 1990; van de Kamp and Leake, 1994; Koeberl et al., 1999; Chan et al., 2000) and are summarized in Table 1. A ThermoNiton XL3-t portable XRF scanner was used to measure 433 samples of protolith, gouge and smear from the R191, Corral Canyon, Courthouse Canyon and Bartlett Wash locations.

As shown on Fig. 9 almost all of the samples from R191 plot above the mean concentration of Sr + Ba (704 ppm), and twenty one gouge and smear samples plot above the maximum background value (1309 ppm), indicating that gouge is enriched in Sr + Ba at this location. Sr + Ba values for Corral Canyon, Courthouse Canyon and Bartlett wash generally plot between the mean and maximum background concentrations, but there is not enrichment of Sr + Ba in the fault rocks relative to protolith at those locations. All locations have significant populations of gouge, smear and protolith samples that plot above the maximum background concentration for Cu + Pb + Zn (182 ppm), suggesting that all locations were exposed to the Oligocene fluid flow event. At Bartlett Wash most gouge samples plot above that maximum, with the concentrations as great as 775 ppm. This indicates enrichment of Cu + Pb + Zn in gouge relative to smear and protolith at Bartlett Wash.

At both R191 and Bartlett Wash gouge is enriched in Ti relative to protolith and smear (Fig. 10). At R191 a large portion of gouge samples plot above the background maximum of 5376 ppm. At Bartlett Wash seven gouge samples plot above the background maximum. No enrichments in Ti in fault rocks relative to protolith are observed at Corral Canyon or Courthouse Canyon, although eight protolith samples at Corral Canyon plot above the background maximum. Gouge, smear and protolith at R191 have large populations with potassium concentrations above the maximum background of 45,157 ppm, with gouge enriched relative to smear and protolith. Gouge is enriched in K relative to protolith at Bartlett Wash, but only one value plots above the maximum background. A significant number of gouge, protolith and smear samples from

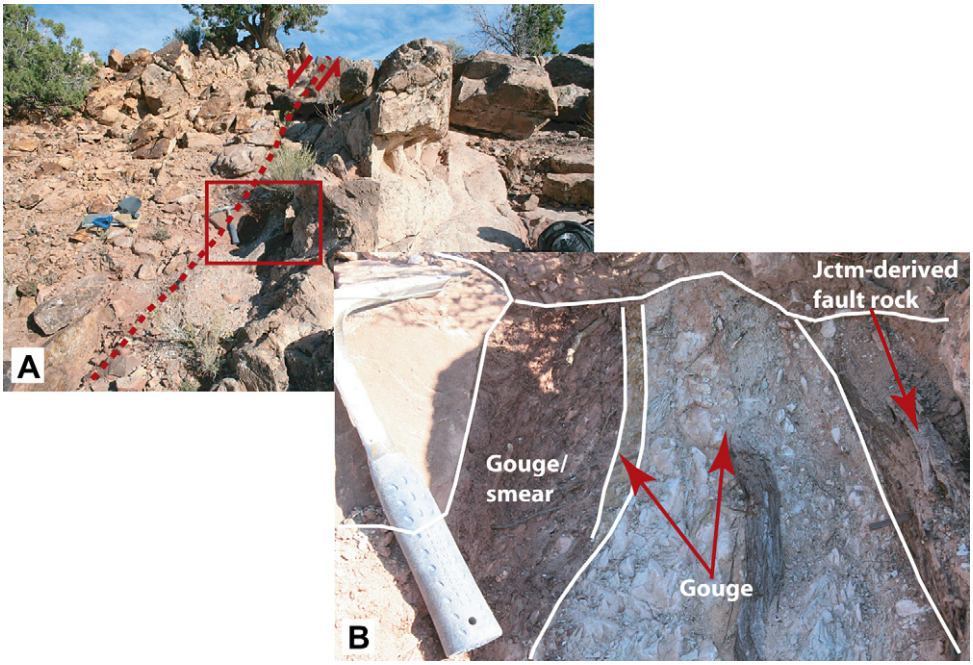

Fig. 8. Closer view of the minor gouge at Bartlett Wash. As at other locations there are both shale smear and clay gouge present at this location.

Corral Canyon plot above the maximum background, but there is no enrichment in fault rocks relative to protolith. Only one point from Courthouse Canyon is above the background maximum and there is no distinction between gouge, smear and protolith.

3.3. Friction tests and scanning electron microscopy

Coefficients of friction were measured by disaggregating rock samples, mixing the disaggregated sample with distilled water to create a slurry, and spreading a 1 mm thick layer of that slurry between two saw-cut forcing blocks of Berea sandstone. Samples were run using an effective confining stress of 40 MPa (10 MPa pore pressure) and sliding rates of 0.01, 0.1, and 1 μm/s in order to allow the rate dependence of the coefficient of friction to be measured.

The coefficients of sliding friction for clay-rich samples from the R191 exposure are shown in Fig. 11. Sand-rich samples (sandstone in the Cutler formation, Moab tongue, and Salt Wash formation) were not run, and are assumed to have coefficients of friction of ~0.6–0.85, compatible with Byerlee's law (e.g., Byerlee, 1978). Values in shale from the Cutler are ~0.44–0.46, ranging from ~0.47 to 0.41 in the Cutler-derived smear, and from ~0.34 to 0.41 in gouge along the major fault. Gouge along the minor fault ranges from 0.25 to 0.43. The values in the Moenkopi-derived smear are 0.4–0.44, and values in the Salt Wash are highly heterogeneous ranging from 0.27 to 0.46.

The rate dependence of all samples is positive. Values range from ~0.006 to 0.008 in shale from the Cutler formation, from 0.0052 to 0.0096 in Cutler-derived smear, from 0.0064 to 0.012 in

Table 1
Compilation of published compositional data for the Paradox Basin.

Formation	Fe (ppm)	K (ppm)	Ti (ppm)	Sr (ppm)	Ba (ppm)	Cu (ppm)	Pb (ppm)	Zn (ppm)	Source
Salt Wash, whole rock	–	–	–	49	340	–	–	–	Breit et al., 1990
Salt Wash, whole rock	–	–	–	58	280	–	–	–	Breit et al., 1990
Salt Wash, whole rock	–	–	–	120	260	–	–	–	Breit et al., 1990
Salt Wash, whole rock	–	–	–	65	240	–	–	–	Breit et al., 1990
Summerville-Tidwell, whole rock of iron oxides	2728.05	2656.32	327.25	446	1300	–	–	–	Chan et al., 2000
Navajo, whole rock of iron oxides	230,135.5	9297.12	140.25	24	190	–	–	–	Chan et al., 2000
Slick Rock, whole rock of iron oxides	200,057	8716.05	187	67	420	–	–	–	Chan et al., 2000
Chinle 1, whole rock	12,031.4	14,028.69	2290.75	97	678	2	–	22	Koeberl et al., 1999
Chinle 2, whole rock	10,212.7	26,646.21	2337.5	140	348	2	–	24	Koeberl et al., 1999
Cutler, whole rock	3567.45	7055.85	1168.75	33	226	2	–	16	Koeberl et al., 1999
Kayenta, whole rock	7204.85	29,468.55	5376.25	67	454	2	–	55	Koeberl et al., 1999
Moenkopi, whole rock	17,627.4	17,598.12	2711.5	140	980	2	–	40	Koeberl et al., 1999
Navajo, whole rock	2867.95	18,677.25	1122	62	347	2	–	11	Koeberl et al., 1999
Wingate, whole rock	8114.2	20,669.49	1776.5	81	416	2	–	18	Koeberl et al., 1999
Cutler, whole rock	13,384.14	25,484.07	1075.25	158	713	11	13	37	van de Kamp and Leake, 1994
Cutler, whole rock	25,594.07	23,906.88	2244	258	1051	15	19	47	van de Kamp and Leake, 1994
Cutler, whole rock	19,912.86	17,930.16	1355.75	199	963	10	13	37	van de Kamp and Leake, 1994
Cutler, whole rock	20,511.57	32,207.88	1823.25	116	900	10	25	35	van de Kamp and Leake, 1994
Cutler, whole rock	18,925.77	25,318.05	1542.75	176	877	11	17	39	van de Kamp and Leake, 1994
Cutler, whole rock	33,724.65	22,578.72	3085.5	165	494	25	19	88	van de Kamp and Leake, 1994
Cutler, whole rock	55,750.95	31,045.74	3833.5	128	598	35	20	127	van de Kamp and Leake, 1994
Cutler, whole rock	48,561.84	45,157.44	3085.5	167	594	55	17	92	van de Kamp and Leake, 1994

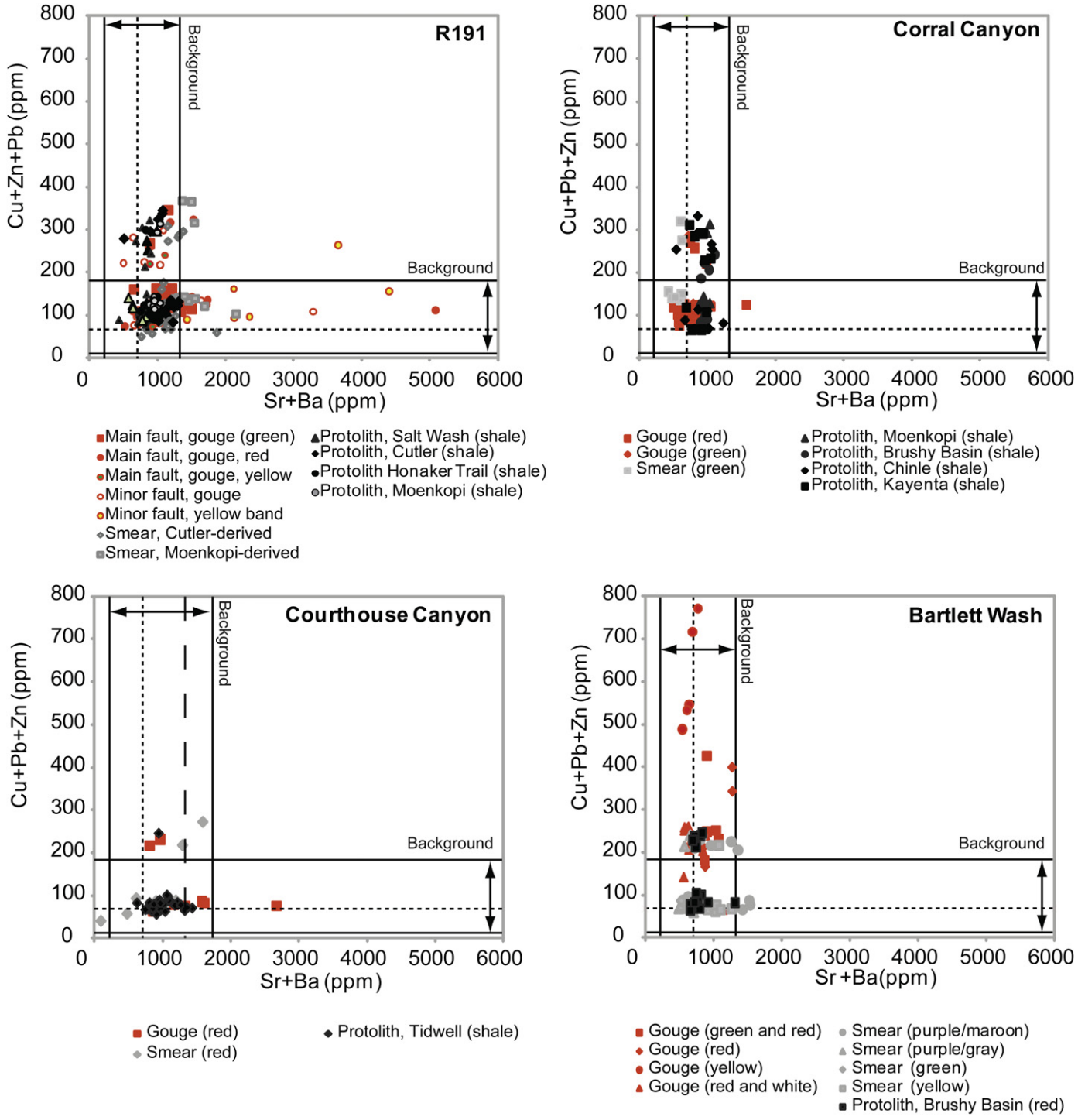

Fig. 9. XRF data for all locations showing Ba + Sr vs. Cu + Pb + Zn concentrations. Ba + Sr concentrations are related to a Paleocene episode of fluid flow while Cu + Pb + Zn concentrations are associated with an Oligocene episode of fluid flow.

clay gouge from the major fault, from 0.0034 to 0.0088 in clay gouge from the minor fault, from 0.0056 to 0.0092 in Moenkopi-derived smear, and from 0.0056 to 0.0104 in shale from the Salt Wash member.

Plucked samples of slip surfaces from the R191 location were analyzed using a scanning electron microscope (SEM) with a secondary electron (SE) detector. Slip surfaces from samples used for friction tests were also analyzed to allow for comparison with their natural equivalents. SEM images from R191 show that gouge is composed of both authigenic and detrital components (Fig. 12) and show that high preferred orientation of clays is extremely localized, extending a few 10s of micrometers from the slip surface (Fig. 13). The overall preferred orientation in the samples is low above that scale. This is compatible with published measurements of the clay fabrics at the mm-scale, which showed very poor fabric development above that scale (Solum et al., 2005). *Natural slip surfaces are more continuous than their experimental analogues* (Fig. 14).

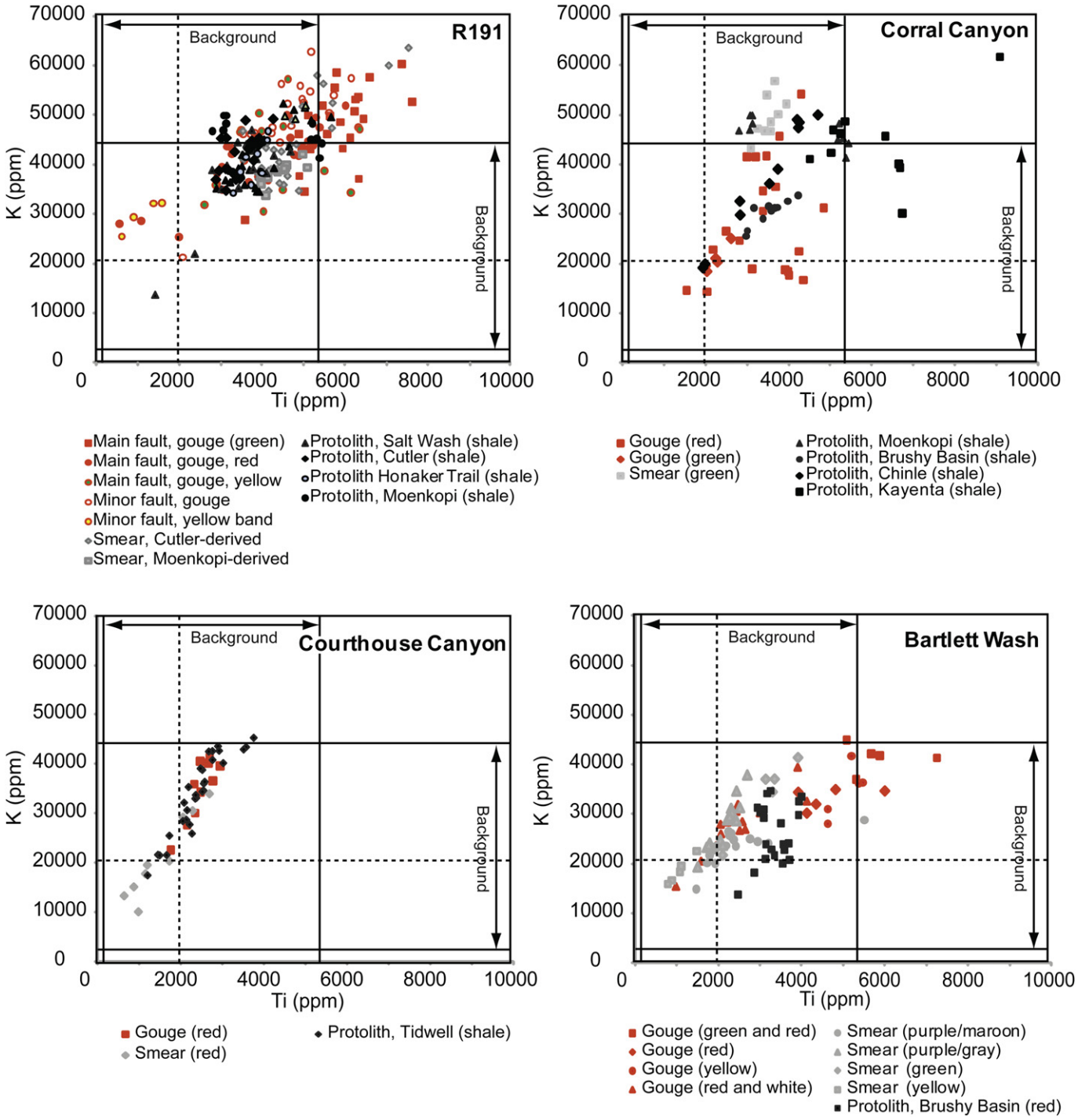

Fig. 10. XRF data for all locations showing K and Ti concentrations. At R191 and Bartlett Wash fault rocks are enriched in K and Ti relative to protolith, indicating enrichment in clays accompanied by the removal of mobile elements. There is no difference between protolith and fault rocks at Corral Canyon and Courthouse Canyon.

4. Discussion

Clay-rich fault rocks, including layers of gouge from 1 cm to 1 m thick are present at R191, Corral Canyon, Courthouse Canyon and Bartlett Wash, along faults with throws of 10 m–~1 km. This indicates that formation of clay-rich fault rocks along the Moab Fault is common.

The mineralogy of the R191 stop is summarized in Fig. 15. Clays in the major gouge are dominated by 70+ wt% 1Md illite with very little mixed-layer illite–smectite. Gouge from the minor fault is heterogeneous, with one value plotting with the major gouge, and two containing <10 wt% 2 M1 illite, but containing 50–70% mixed-layer clays. This value is similar to the composition of clays in the Salt Wash member of the Morrison Formation adjacent to the fault. Clays in the Cutler Group are dominated by 2M1 illite (± muscovite) with between 5–45% mixed-layer illite–smectite. The Cutler-derived smear ranges from ~60 to 80% 2M1 illite with 55–65% mixed-layer clays to 10–20% 2M1 illite with ~30% mixed-layer clays. As discussed in Solum et al. (2005) the discrete 1Md illite in the major gouge is neoformed, and the clays in the smear are

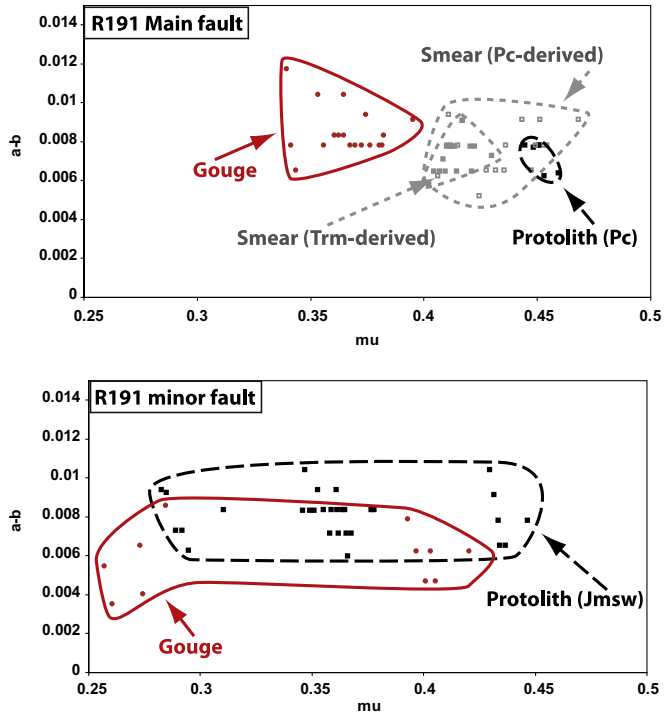

Fig. 11. Coefficients of friction and rate dependence for samples from the R191 location. Note that only clay-rich samples are plotted. Blue symbols are from protolith, green are from shale smear and red are from clay gouge. The coefficient of friction in the Cutler formation (~0.45) is similar to that in the Cutler-derived smear, although there is a decreasing trend toward the gouge. The value in the gouge is 0.35–0.4, indicating that fault-related authigenesis promotes fault zone weakening. The values in the hanging wall protolith (the Salt Wash Member of the Morrison Formation) show considerable scatter, likely due to the presence of bed-parallel slip observed in the field. The higher value of 0.45 likely represents pristine protolith while the lower values are due in part to fault-related authigenesis. The heterogeneity in the minor gouge zone reflects compositional variability (Solum et al., 2005), and indicates that the smaller fault zone is not as well mixed as the larger. Changes in the rate dependence of the coefficient of friction suggest that the authigenesis in the major gouge zone promotes stable sliding behavior (compatible with observations that the authigenesis consists of the formation of illite) and may enhance the possibility of stick-slip behavior in the minor gouge zone (compatible with the observation that the authigenesis at this location is dominated by the formation of illite–smectite).(For interpretation of the references to colour in this figure legend, the reader is referred to the web version of this article.)

forming through the alteration of detrital illite/muscovite in the Cutler Group.

The enrichment in K and Ti in gouge relative to protolith at R191 indicates that gouge is enriched in clays. The enrichment in Ti, an immobile element, relative to protolith, coupled with the observation

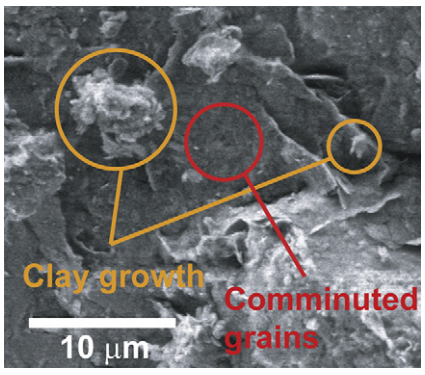

Fig. 12. SEM images of gouge from R191 showing authigenic clays filling pores and coating surfaces that are comprised of comminuted grains.

that the Ti concentration in the gouge is greater than the background maximum, indicates that the clay enrichment is associated with the removal of more mobile elements. In addition, it is possible to qualitatively distinguish illite from mixed-layer illite–smectite through examination of K and Ti. A compilation of published K and Ti compositions of 2M1 illite (Post and Borer, 2002; Fleet, 2003), 1Md illite (McLaughlin, 1958; Clay Minerals Society, 2010) and mixed-layer illite–smectite (Eberl et al., 1987; Mermut and Cano, 2001; McCarty and Reynolds, 1995; Lynch et al., 1997; Underwood and Deng, 1997; Srodon et al., 2009; Clay Minerals Society, 2010) is shown in Fig. 16.

The Ti and K concentrations from the R191 locality can be compared to the reference compilation if those values are adjusted to account for dilution of clay-related elemental concentrations by non-clays phases such as quartz. The mineralogy of R191 samples is given in Table 2. The mineral concentrations shown in Table 2 were used to crudely account for the dilution of Ti and K by non-clay phases. This correction allows the elemental concentrations from R191 to be qualitatively compared to the elemental concentrations for 2M1 illite, 1Md illite, and mixed-layer illite–smectite shown in Fig. 16. While there is considerable overlap between fault rocks and protolith, more of the protolithic points plot in the 2M1 illite field, and more of the fault rocks (gouge and smear) plot in the 1Md illite and mixed-layer illite–smectite field. This indicates that the changes in Ti and K concentrations from XRF are related to the mineralogical changes inferred from XRD. The enrichment in Ba + Sr in fault rocks relative to protolith at R191 indicates that the fluid responsible for the relative enrichment in Ti was the Paleocene fluid associated with hydrocarbon migration and a period of major fault activity.

Fault rocks at both Corral Canyon and Courthouse Canyon do not show enrichment in Ti or K relative to protolith, indicating that fault rocks are not enriched in clays relative to protolith at those locations, and suggesting that authigenesis at those locations is minor, and therefore that formation of the clay-rich fault rocks at those locations is dominated by mechanical processes. It is important to note that the Courthouse Canyon location described in this paper is not the same as the one in between the main and northern branches of the Moab Fault that exhibits a high density of calcite veins (Foxford et al., 1996; Davatzes et al., 2005a,b; Davatzes and Aydin, 2005; Eichhubl et al., 2009). Fault rocks at Bartlett Wash show an enrichment in Ti and K relative to protolith, indicating that fault rocks at that location are enriched in clays relative to protolith, similar to the R191 locality. Given the similarity in patterns of Ti and K concentrations at R191 and Bartlett Wash it is possible that authigenesis is active at both locations, but this cannot be conclusively confirmed without XRD. Since fault rocks at Bartlett Wash are enriched in Cu + Pb + Zn relative to protolith it appears that the fluid responsible for the elemental changes was the Oligocene fluid associated with igneous activity in the La Sal Mountains, and possibly with a period of activity along the northern section of the Moab Fault and the Little Grand Wash Fault to the NW.

There are populations of samples at R191, Corral Canyon and Courthouse Canyon that have Cu + Pb + Zn concentrations that are greater than the background maximum, but those populations are composed of both fault rock and protolith. Morrison and Parry (1986) note the spatial association of faults with copper ore deposits in the Lisbon Valley to the south of Moab, and they relate that observation to the migration of mineralizing fluids along those faults. The XRF data suggest that this fluid moved along the Moab Fault at all of the four locations sampled in this study, however only at Bartlett Wash are fault rocks enriched in Cu + Pb + Zn relative to protolith. This suggests that only the Bartlett Wash section of the fault was active at this time. As discussed above, fault rocks at Bartlett Wash are enriched in clays relative to protolith, and since

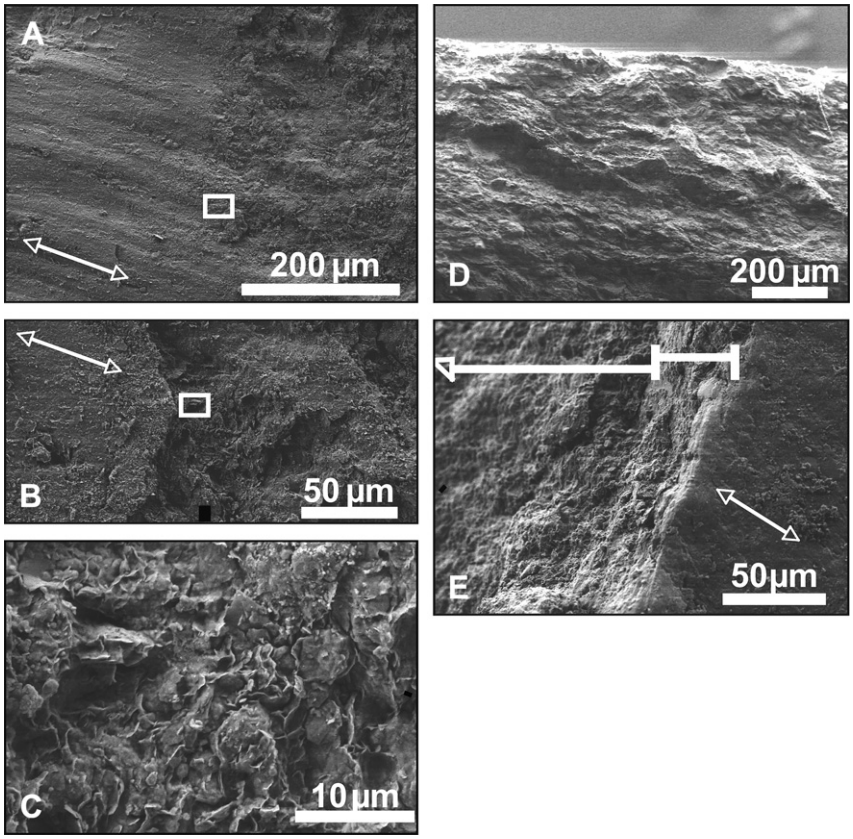

Fig. 13. SEM images of slip surfaces from smear and gouge from R191. A) Map view of slip surface from shale smear derived from the Cutler formation showing discontinuous nature of slip patches. Double arrow shows slickenline orientation. Note that the slickenline texture is not present in the right half of the image. Box denotes region shown in B. B) Closer view of slip surface shown in A. Note that the slip surface is extremely thin and is underlain by clays with a low degree of preferred orientation exhibiting an open edge-to-face geometry. Box denotes area shown in C. C) Closer view of edge-to-face geometry underlying slip surface in the shale smear. D) Cross-sectional and E) Oblique view of a slip surface from clay gouge from the major gouge zone. Note that Preferred orientation is limited to the region within a few 10s of micrometers from the slip surface. The clays outside that range how a low degree of preferred orientation.

this enrichment occurred in the presence of a Cu + Pb + Zn-bearing fluid the fault rocks are enriched in that suite of elements. Similarly, since the enrichment in clays in fault rocks at R191 occurred in the presence of a Ba + Sr-bearing fluid, those fault rocks are enriched in Ba + Sr relative to protolith.

There are two significant implications to the presence of fault-related authigenesis along the fault. The first is that estimates of fault rock composition based on the SGR or CSP algorithms do not account for fault-related neoformation of clays, which is responsible for the formation of much of the clay at R191 and likely at Bartlett Wash. Improving estimates of fault rock composition, and in the presence of authigenesis the mechanisms that maintain clay gouge continuity, therefore require that fault-related authigenesis be constrained. Since these estimates are used to estimate fault rock permeability and/or extent quantifying fault-related authigenesis has direct implications for quantifying the hydrologic properties of faults. Second, clay authigenesis, as evidenced by the comparison of synthetic and natural clay gouges (Fig. 14), enhances the membrane sealing potential of slip surfaces in clay gouge by filling already small pore throats, although this phenomenon has yet to be quantified, and must therefore be regarded as somewhat speculative.

The SEM observations show that the degree of preferred orientation in the gouge is generally low, with high preferred orientation extending at most a few 10s of micrometers from a slip surface. This is supported by mm-scale characterizations of gouge from the R191 stop which indicate the fabric at that location is up

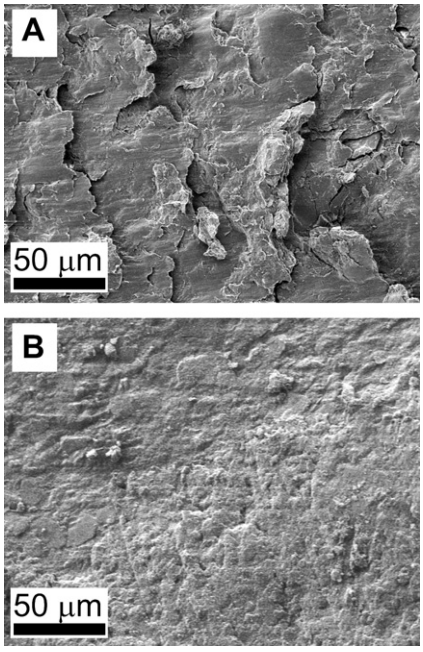

Fig. 14. SEM images of a natural slip surface (A) from gouge from R191 and a synthetic slip surface (B) created during a friction test on the same gouge sample. The natural slip surface is the product of both mechanical and authigenic processes while the synthetic slip surface is solely the product of mechanical processes. The more continuous nature of the natural slip surface indicates that fault-related authigenesis enhances slip surface continuity and potentially seal capacity.

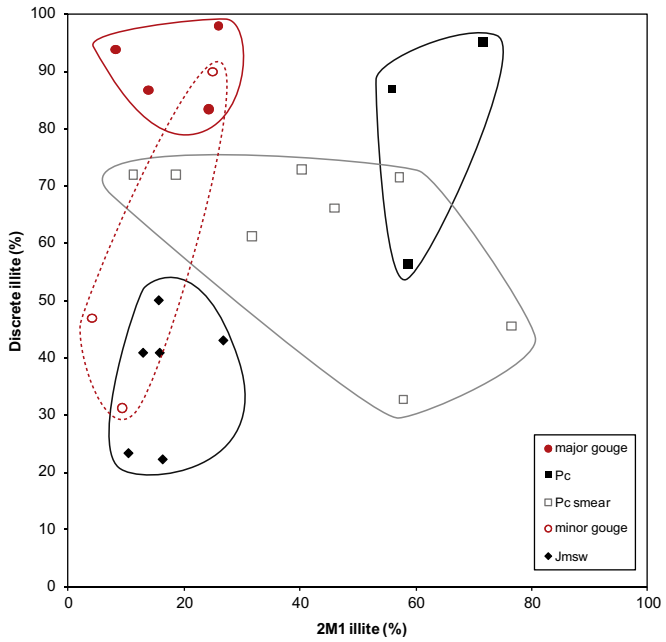

Fig. 15. Clay mineralogy at the R191 location. The major gouge is enriched in authigenic 1Md illite relative to protolith, while smear is heterogeneous, but dominated by the formation of mixed-layer illite–smectite.

to ~2.5 times more intense in protolith than in fault rocks, despite the presence of a macroscopic foliation in the gouge (Solum et al., 2005). This is significant because it suggests that the mechanical behavior of the fault can be influenced by processes that occur below the mm.

The comparison of the natural and synthetic slip surfaces indicates that clay authigenesis promotes slip surface continuity, and indicates that authigenesis is common along slip surfaces consistent with increased change in mineral and elemental composition in the most well developed clay gouge where slip surfaces are relatively abundant. As discussed above a layer of clay gouge was observed at each of the locations described in this study, and these zone contain both bounding and internal slip surfaces. This is compatible with studies of other faults, notably the San Andreas Fault where clay authigenesis is also common as revealed by studies extracted from the SAFOD borehole (Solum et al., 2006). In this circumstance, the authigenic clays occur as thin coatings on slip surfaces (Schleicher et al., 2006), and lead to a reduction in the coefficient of friction (Tembe et al., 2006; Morrow et al., 2007).

Authigenesis also has the ability to affect the frictional properties of the Moab Fault. At the R191 location the coefficient of friction in the Cutler-derived smear decreases toward the main gouge zone culminating in a significantly low value in the main gouge zone as compared to either the adjacent smear or the protolithic Cutler formation. Moreover, the frictional properties of the main gouge zone are more homogeneous than in the Cutler-derived smear or in undeformed Cutler since both of those contain interbedded

Table 2
XRD data for the R191 location.

	Kaolinite (%)		Quartz (%)		Microcline (%)		Albite (%)		Illite + I-S	
	Average	Std. Dev.	Average	Std. Dev.	Average	Std. Dev.	Average	Std. Dev.	Average	Std. Dev.
Minor gouge	13	7	7	5	4	5	12	15	64	8
Major gouge	14	8	33	8	8	4	0	1	44	8
Smear	14	10	10	10	10	8	0	0	67	11
Protolith	6	4	22	19	15	14	4	1	53	1

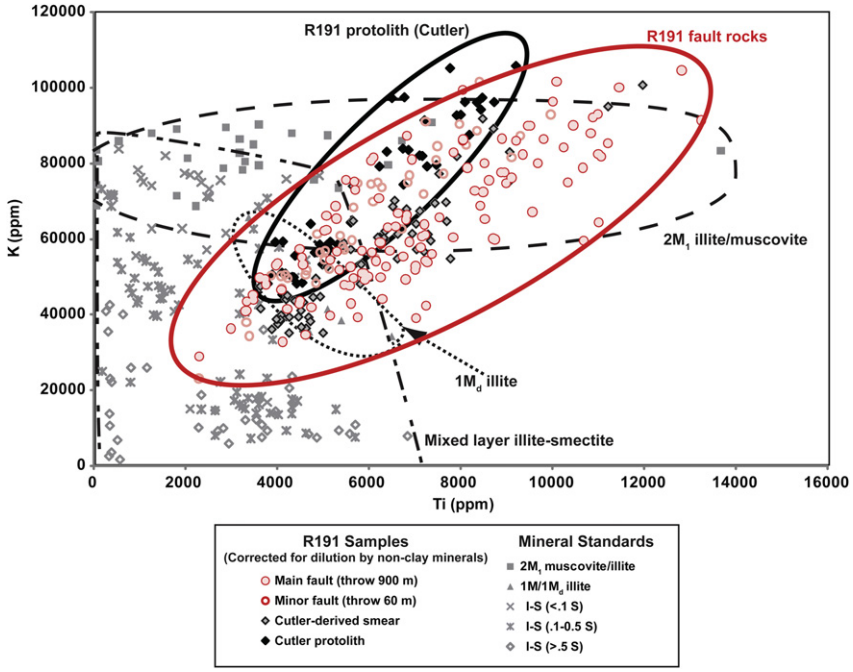

Fig. 16. K and Ti concentrations at R191 adjusted for dilution by non-clay phases. A compilation of K and Ti concentrations for 2M1 illite, 1Md illite and mixed-layer illite–smectite ranging from highly illitic to highly smectitic are plotted as gray symbols. Sources for reference minerals are as follows: 2M1 illite (Post and Borer, 2002; Fleet, 2003); 1Md illite (McLaughlin, 1958; Clay Minerals Society, 2010); mixed-layer illite-smectite (Eberl et al., 1987; Mermut and Cano, 2001; McCarty and Reynolds, 1995; Lynch et al., 1997; Underwood and Deng, 1997; Srodon et al., 2009; Clay Minerals Society, 2010).

sandstones and shales. Unlike the main gouge zone the coefficients of friction from the minor gouge zone are heterogeneous compatible with a heterogeneous mineralogical composition which includes one population of clays resembling the clays in the adjacent Salt Wash member and another population that was interpreted to be fault-related (Solum et al., 2005). The more protolithic clays in the minor gouge (mixed-layer illite–smectite) are stronger than the fault-related clays (very smectite-rich illite–smectite).

Changes in the coefficient of friction of the gouge can be important when considering fluid leakage associated with seismic rupture. Wilkins and Naruk (2007) estimate the volume of fluid loss caused by leakage associated with coseismic dilational pulses. They found that the slip rate of a fault strongly influenced the cumulative fluid loss since a lower slip rate implies fewer earthquakes and therefore fewer coseismic dilational pulses. For faults experiencing fault valve behavior (Sibson, 1990), an increased coefficient of friction means that it will take longer for failure to occur because it will take longer for sufficient fluid pressure to develop, assuming a Mohr–Coulomb failure criterion. Similarly, a reduction in the coefficient of friction means that failure will occur more often. This may mean that an increased coefficient of friction will reduce the volume of fluid loss associated with coseismic dilation, and vice versa for a decreased coefficient of friction.

Wilkins and Naruk (2007) also note that volume loss will be substantially less for an aseismically creeping fault than for its seismic equivalent. This means that if authigenesis causes a change in the style of failure of a fault, then the volume of fluid lost along that fault will change. If an aseismic fault becomes seismic then the volume loss will increase, and if a seismic fault becomes aseismic then the volume loss will decrease (all other parameters held constant). At slower slip rates, the ductile nature of clay revealed by slip surface striations bending around asperities on the fault surface likely minimize dilation that could lead to increased permeability (Davatzes and Hickman, 2005). Reducing coefficients of friction associated with clay authigenesis mean that relatively small variations in shear stress can locally produce a new slip vector, thus promoting this dilation minimizing behavior. Lockner et al. (2006) propose that it may be easier to have seismic rupture in montmorillonite-rich gouge than in illite-rich gouge since the rate dependence in montmorillonite gouge is neutral to slightly negative as opposed to markedly positive in illite gouge. The rate dependence of all of the samples measured in this study was positive, however all of these samples used distilled water as a pore fluid. Lockner et al. (2006) found that the rate dependence of montmorillonite in distilled water was -0.0002 ± 0.0002, decreasing to -0.0008 ± 0.0003 in a 1 M KCl brine. Since the Moab Fault is related to movement of an underlying salt deposit and interacted with migrating oil sourced in or below this salt (Nuccio and Condon, 1996; Garden et al., 2001), the water that moved along it was most likely a brine, indicating that the rate dependence of the minor gouge may have been negative.

5. Conclusions

Clay gouge and shale smear are common along the Moab Fault, with clay gouges ranging in thickness from ~1 cm to ~1 m. Fault-related clay authigenesis at the R191 location is accompanied by an increased concentration of K, Ti and Ba + Sr in fault rocks relative to protolith indicating enrichment of clays in fault rocks in the presence of a Paleocene Ba + Sr-bearing fluid. Fault rocks at Bartlett Wash are also enriched in K and Ti, suggesting enrichment of clays in fault rocks relative to protolith. These fault rocks are also enriched in Cu + Pb + Zn relative to protolith, indicating that the clay enrichment occurred in the presence of an Oligocene Cu + Pb + Zn bearing fluid. Fault rocks from Corral Canyon and Courthouse Canyon show little if any difference in composition relative to protolith, suggesting that fault rock formation at those locations is governed by mechanical as opposed to authigenic processes. Reasons for the prevalence of authigenic processes at R191 and Bartlett Wash and their paucity at Corral Canyon and Courthouse Canyon are not clear.

The continuity of the slip surfaces at the R191 location is enhanced by authigenesis, and strong preferred orientation of clays occurs only within a few 10s of micrometers of the slip surface promoting membrane sealing in addition to low permeability across the fault. These results suggest that fault behavior can be significantly affected by authigenesis in locations where authigenesis is common, although the magnitude of authigenesis-related changes in mechanical and hydrologic properties has yet to be quantified.

Acknowledgements

Funding for this work was provided by the U.S. Geological Survey Mendenhall Program (Solum, Davatzes) and Shell International Exploration and Production (Solum, Davatzes) and Sam Houston State University (Solum). The use of the XL3-t device was graciously provided by ThermoNiton. The authors thank management at Shell for permission to publish and Brent Couzens-Schultz, Alan Morris, and an anonymous reviewer are thanked for their reviews of an earlier version of the manuscript.

References

Anyamele, N., Davatzes, N.C, Solum, J., 2009. Characterizing clay gouge formation and implications for fault zone permeability, Moab Fault, Utah. In: American Association of Petroleum Geologists Annual Meeting, AAPG Search and Discovery Article #90090.

Aydin, A., Eyal, Y., 2002. Anatomy of a normal fault with shale smear: implications for fault seal. AAPG Bulletin 86 (8), 1367–1381.

Breit, G.N., Goldhaber, M.B., Shawe, D.R., Simmmons, E.C., 1990. Authigenic barite as an indicator of fluid movement throught sandstones within the Colorado Plateau. Journal of Sedimentary Petrology 60, 884–896.

Bretan, P., Yielding, G., Jones, H., 2003. Using calibrated shale gouge ratio to estimate hydrocarbon column heights. AAPG Bulletin 87, 397–413. doi:10.1306/08010201128.

Byerlee, J., 1978. Friction of rocks. Pure and Applied Geophysics 166, 615–625.

Caine, J.S., Evans, J.P., Forster, C.B., 1996. Fault zone architecture and permeability structure. Geology 24, 1025–1028.

Chan, M.A., Parry, W.T., Bowman, J.R., 2000. Diagenetic hematite and manganese oxides and fault-related fluid flow in Jurassic Sandstones, Southeastern Utah. AAPG Bulletin 84, 1281–1310.

Chan, M.A., Parry, W.T., Petersen, E.U., Hall, C.M., 2001. $^{40}Ar/^{39}Ar$ age and chemistry of manganese mineralization in the Moab and Lisbon fault systems, southeastern Utah. Geology 29, 331–334.

Childs, C., Manzocchi, T., Walsh, J.J., Bonson, C.G., Nicol, A., Schopfer, M.P.J., 2009. A geometric model of fault zone and fault rock thickness variations. Journal of Structural Geology 31, 117–127.

Crawford, B.R., Myers, R.D., Woronow, A., Faulkner, D.R., Rutter, E.H., 2002. Porosity-permeability Relationships in Clay-bearing Fault Gouge, SPE/ISRM 78214, 13 pp.

Davatzes, N.C., Hickman, S.H., 2005. Comparison of acoustic and electrical image logs from the Coso Geothermal Field, CA. In: 30th Stanford University Workshop on Geothermal Reservoir Engineering, 01/ 31-02/2, 2005, SGP-TR-176, p. 11.

Davatzes, N.C., Aydin, A., 2005. Distribution and nature of fault architecture in a layered sandstone and shale sequence: an example from the Moab Fault, Utah. In: Sorkhabi, R., Tsuji, Y. (Eds.), Faults, Fluid Flow and Petroleum Traps. AAPG Memoir, vol. 85, pp. 153–180.

Davatzes, N.C., Eichhubl, P., Aydin, A., 2005a. Structural evolution of fault zones in sandstone by multiple deformation mechanisms: Moab Fault, SE Utah. GSA Bulletin 117, 135–148.

Davatzes, N.C., Solum, J., Lockner, D., Stanchits, S., 2005b. Fault rock generation, frictional properties, and permeability in fault rocks of the Moab Fault, Utah. Geological Society of America Abstracts with Programs 37 (7), 498.

Doelling, H.H., 2001. Geologic Map of the Moab and Eastern Part of the San Rafael Desert 300!600 Quadrangles, Grand and Emery Counties, Utah and Mesa County, Colorado. In: Geologic Map 180: Utah Geological Survey Geologic Map 180, Scale 1:100,000.

Eberl, D.D., Srodon, J., Lee, M., Nadeau, P.H., Northrop, H.R., 1987. Sericite from the Silverton caldera, Colorado: correlation among structure, composition, origin, and particle thickness. American Mineralogist 72, 914–934.

Eichhubl, P., Davatzes, N.C., Becker, S.P., 2009. Structural and diagenetic control of fluid migration and cementation along the Moab Fault, Utah. AAPG Bulletin 93, 653–681. doi:10.1306/02180908080.

Eichhubl, P., D'Onfro, P.S., Aydin, A., Waters, J., McCarty, D.K., 2006. Structure, petrophysics, and diagenesis of shale entrained along a normal fault at Black Diamond Miners, California—implications for fault seal. AAPG Bulletin 89, 1113–1137.

Faulkner, D.R., Rutter, E.H., 2001. Can the maintenance of overpressured fluids in large strike-slip fault zones explain their apparent weakness? Geology 29, 503–506.

Fisher, Q.J., Knipe, R.J., 2001. The permeability of faults within siliciclastics petroleum reservoirs of the North Sea and Norwegian Continental Shelf. Marine and Petroleum Geology 18, 1063–1081.

Fleet, M.E., 2003. Rock-Forming minerals. In: Deer, W.A., Howie, R.A., Zussman, J. (Eds.), Sheet Silicates: MicasGeological Society of London, second ed., vol 3A, p. 758.

Foxford, K.A., Garden, I.R., Guscott, S.C., Burley, S.D., Lewis, J.J.M., Walsh, J.J., Watterson, J., 1996. The field geology of the Moab Fault. In: Huffman Jr, A.C., Lund, W.R., Goodwin, L.H. (Eds.), Geology and Resources of the Paradox Basin. Utah Geological Association Guidebook, vol. 25, pp. 265–283. Salt Lake City.

Foxford, K.A., Walsh, J.J., Watterson, J., Garden, I.R., Guscott, S.C., Burley, S.D., 1998. Structure and content of the Moab Fault zone, Utah, USA, and its implications for fault seal prediction. In: Jones, G., Fisher, Q.J., Knipe, R.J. (Eds.), Faulting, Fault Sealing and Fluid Flow in Hydrocarbon Reservoirs. Geological Society of Special Publication, vol. 147, pp. 87–103.

Fulljames, J.R., Zijerveld, L.J.J., Franssen, R.C.M.W., 1997. Fault seal processes: systematic analysis of fault seals over geological and production time scales. In: Moller-Pederson, P., Koestler, A.G. (Eds.), Hydrocarbon Seals: Importance for Exploration and Production. Norwegian Petroleum Society Special Publication, vol. 7, pp. 51–59.

Garden, I.R., Guscott, S.C., Burley, S.D., Foxford, K.A., Walsh, J.J., Marshall, J., 2001. An exhumed palaeo-hydrocarbon migration fairway in a faulted carrier system, Entrada Sandstone of SE Utah, USA. Geofluids 1, 195–213.

Johansen, T.E.S., Fossen, H., Kluge, R., 2005. The impact of syn-kinematic porosity reduction on damage zone architecture in porous sandstone; an outcrop example from the Moab Fault, Utah. Journal of Structural Geology 27, 1469–1485.

Koeberl, C., Plescia, J.B., Hayward, C.L., Reimold, W.U., 1999. A petrographical and geochemical study of quartzose nodules, country rocks, and dike rocks from the Upheaval Dome structure, Utah. Meteoritics and Planetary Science 34, 861–868.

Knipe, R.J., Jones, G., Fisher, Q.J., 1998. Faulting, fault sealing and fluid flow in hydrocarbon reservoirs: an introduction. In: Jones, G., Fisher, Q.J., Knipe, R.J. (Eds.), Faulting, Fault Sealing and Fluid Flow in Hydrocarbon Reservoirs. Geological Society, London, Special Publications, vol. 147, pp. vii–xxi.

Lockner, D., Solum, J.G., Davatzes, N., 2006. The effect of brine composition and concentration on strength of expandable clays. Eos Transactions AGU 87 (52) Fall Meet. Suppl., Abstract T31F-03.

Lynch, F.L., Mack, L.E., Land, L.S., 1997. Burial diagenesis of illite/smectite in shales and the origins of authigenic quartz and secondary porosity in sandstones. Geochimica et Cosmochimica Acta 61, 1995–2006.

Manzocchi, T., Walsh, J.J., Nell, P., Yielding, G., 1999. Fault transmissibility multipliers for flow simulation models. Petroleum Geoscience 5, 53–63.

McCarty, D.K., Reynolds, R.C., 1995. Rotationally disordered illite/smectite in Paleozoic K-bentonites. Clays and Clay Minerals 43, 271–284.

McLaughlin, R.J.W., 1958. Geochemical partition in two illitic clays. Geochimica et Cosmochimica Acta 15, 165–169.

Mermut, A.R., Cano, A.F., 2001. Baseline studies of the clay minerals society source clays: chemical analyses of major elements. Clays and Clay Minerals 49, 381–386.

Morrison, S.J., Parry, W.T., 1986. Formation of carbonate-sulfate veins associated with copper ore deposits from saline basin brines, Lisbon Valley, Utah: fluid inclusion and isotopic evidence. Economic Geology 81, 1853–1866.

Morrow, C., Solum, J.G., Tembe, S., Lockner, D., Wong, T. –f., 2007. Using drill cuttings separates to estimate the strength of narrow shear zones at SAFOD. Geophysical Research Letters 34 (L11301). doi:10.1029/2007GL029665.

Nuccio, V.F., Condon, S.M., 1996. Burial and Thermal History of the Paradox Basin, Utah and Colorado, and Petroleum Potential of the Middle Pennsylvanian Paradox Basin. U.S. Geologic Survey, Report B 2000-O, pp. O1–O41.

Pevear, D.R., Vrolijk, P.J., Longstaffe, F.J., 1997. Timing of Moab Fault displacement and fluid movement integrated with burial history using radiogenic and stable isotopes. In: Hendry, J., Carey, P., Parnell, J., Ruffell, A., Worden, R. (Eds.), Geofluids II '97: Contributions to the Second International Conference on Fluid Evolution. Migration and Interaction in Sedimentary Basins and Orogenic Belts, Belfast, pp. 42–45.

Post, J.L., Borer, L., 2002. Physical properties of selected illites, beidellites and mixed-layer illite-beidellites from southwestern Idaho, and their infrared spectra. Applied Clay Science 22, 77–91.

Saffer, D.M., Marone, C., 2003. Comparison of smectite- and illite-rich gouge frictional properties: application to the updip limit of the seismogenic zone along subduction megathrusts. Earth and Planetary Science Letters 215, 219–235.

Schleicher, A.M., van der Pluijm, B.A., Solum, J.G., Warr, L.N., 2006. Origin and significance of clay-coated fractures in mudrock fragments of the SAFOD borehole. Geophysical Research Letters 33 (L16313). doi:10.1029/2006GL026505.

Sibson, R.H., 1990. Conditions for fault-valve behaviour. In: Knipe, R.J., Rutter, E.H. (Eds.), Deformation Mechanisms, Rheology and Tectonics. Geological Society Special Publication, vol. 54, pp. 15–28.

Solum, J.G., van der Pluijm, B.A., 2007. Reconstructing the Snake River–Hoback River Canyon section of the Wyoming thrust belt through direct dating of clay-rich fault rocks. Special paper 433: Whence the Mountains? Inquiries into the evolution of orogenic systems: a volume in Honor of Raymond A. Geological Society of America 433 (0), 183–196.

Solum, J.G., van der Pluijm, B.A., 2009. Quantification of fabrics in clay gouge from the Carboneras fault, Spain and implications for fault behavior. Tectonophysics 475, 554–562.

Solum, J.G., Hickman, S.H., Lockner, D.A., Moore, D.E., van der Pluijm, B.A., Schleicher, A., Evans, J.P., 2006. Mineralogical characterization of protolith and fault rocks from the SAFOD main hole. Geophysical Research Letters 33 (L21314). doi:10.1029/2006GL027285.

Solum, J.G., van der Pluijm, B.A., Peacor, D.R., 2005. Neocrystallization, fabrics and age of clay minerals from an exposure the Moab Fault, Utah. Journal of Structural Geology 27, 1563–1576.

Source Clays Project, Source Clay Physical/Chemical Data, http://www.agry.purdue.edu/cjohnston/sourceclays/chem.htm, [accessed on 11/01/2010].

Sperrevik, S., Gillespie, P.A., Fisher, Q.J., Halverson, T., Knipe, R.J., 2002. Empirical estimation of fault rock properties. In: Koestler, A.G., Hunsdale, R. (Eds.), Hydrocarbon Seal Quantification. NPF Special Publication, vol. 11. Elsevier, Amsterdam, pp. 109–125.

Srodon, J., Zeelmaekers, E., Derkowski, A., 2009. The charge of component layers of illite–smectite in bentonites and the nature of end-member illite. Clays and Clay Minerals 57, 649–671.

Tembe, S., Lockner, D.A., Solum, J.G., Morrow, C., Wong, T.-f., Moore, D.E., 2006. Frictional strength of cuttings and core from SAFOD drillhole phases 1 and 2. Geophysical Research Letters 33 (L23307). doi:10.1029/2006GL027626.

Underwood, M.B., Deng, X., 1997. 1. Clay mineralogy and clay geochemistry in the vicinity of the decollement zone, northern Barbados Ridge. In: Shipley, T.H., Ogawa, Y., Blum, P., Bahr, J.M. (Eds.), Proceedings of the Ocean Drilling Program. Scientific Results, vol. 156, pp. 3–30.

van de Kamp, P.C., Leake, B., 1994. Petrology, geochemistry, provenance, and alteration of Pennsylvanian-Permian arkose, Colorado and Utah. GSA Bulletin 105, 1571–1582.

van der Pluijm, B.A., Hall, C.M., Vrolijk, P.J., Pevear, D.R., Covey, M.C., 2001. The dating of shallow faults in the Earth's crust. Nature 412, 172–175.

van der Pluijm, B.A., Hall, C.M., Pevear, D.R., Solum, J.G., Vrolijk, P.J., 2006. Fault dating in the Canadian Rocky Mountains: evidence for late Cretaceous and early Eocene orogenic pulses. Geology 34, 837–840.

Vrolijk, P., van der Pluijm, B.A., 1999. Clay gouge. Journal of Structural Geology 21, 1039–1048.

Walsh, J., Childs, C., Manzocchi, T., 2002. The incorporation of fault properties in flow models for hydrocarbon migration and reservoir production. In: EAGE 64th Conference & Exhibition, Florence, Italy.

Walsh, J.J., Watterson, J., Heath, A.E., Childs, C., 1998. Representation and scaling of faults in fluid flow models. Petroleum Geoscience 4, 241–251.

Williams, A.P., 2005. Structural analysis of CO2 leakage through the Salt Wash and Little Grand Wash faults from natural reservoirs in the Colorado Plateau, southeastern Utah, MSc thesis, Utah State University, pp. 94.

Wilkins, S.J., Naruk, S.J., 2007. Quantitative analysis of slip-induced dilation with application to fault seal. AAPG Bulletin 91, 97–113.

Yan, Y., van der Pluijm, B.A., Peacor, D.R., 2001. Deformation microfabrics of clay gouge, Lewis Thrust, Canada: a case for fault weakening from clay transformation. In: Holdsworth, R.E., Strachan, R.A., Magloughlin, J.F., Knipe, R.J. (Eds.), The Nature and Tectonic Significance of Fault Zone Weakening. Geological Society Special Publication, vol. 186, pp. 103–112.

Yielding, G., Freeman, B., Needham, D.T., 1997. Quantitative fault seal prediction. AAPG Bulletin 81, 897–917.